Journal of Alloys and Compounds 509 (2011) 9919–9923

Contents lists available at ScienceDirect

Journal of Alloys and Compounds

journal homepage: www.elsevier.com/locate/jallcom

Efficient first-order resonant near-infrared quantum cutting in β-$NaYF_4$:Ho^{3+},Yb^{3+}

D.C. Yu, X.Y. Huang, S. Ye, Q.Y. Zhang*

State Key Laboratory of Physics and Chemistry of Luminescence, and Institute of Optical Communication Materials, South China University of Technology, Guangzhou 510641, PR China

ARTICLE INFO

Article history:
Received 5 July 2011
Accepted 26 July 2011
Available online 4 August 2011

Keywords:
Down-conversion
Quantum cutting
Energy transfer
Near-infrared
Solar cells

ABSTRACT

We demonstrated an efficient two-photon near-infrared (NIR) quantum cutting (QC) in Ho^{3+}–Yb^{3+} co-doped hexagonal β-$NaYF_4$, which could efficiently convert an incident high-energy photon in the wavelength region of 300–550 nm into two NIR photons. Underlying mechanism for the two-photon NIR-QC process is analyzed in terms of static and dynamic photoemission and monitored excitation spectra. It is found that NIR-QC can occur through two possible energy transfer (ET) approaches: (i) the excited Ho^{3+}:$^5F_3$ state may simultaneously excite two Yb^{3+} neighbors via a cooperative ET process, and (ii) the NIR-QC can be feasibly induced by a first $Ho^{3+}(^5S_2,^5F_4) + Yb^{3+}(^2F_{7/2}) \rightarrow Ho^{3+}(^5I_6) + Yb^{3+}(^2F_{5/2})$ resonant ET process and a sequential $^5I_6 \rightarrow {}^5I_8$ transition of Ho^{3+}. This novel $NaYF_4$:Ho^{3+},Yb^{3+} NIR-QC phosphor, may explore a new approach to maximize the performance of solar cells.

1. Introduction

Quantum cutting (QC) involving efficient down-conversion of one incident high-energy photon to two or more low-energy photons has become a hot-focused research topic recently [1–3]. It is of very significance to develop novel QC materials with quantum efficiency (QE) exceeding unity. Ever since QC was first achieved in Pr^{3+}-doped fluorides by cutting one incident vacuum ultraviolet (UV) photon into two visible photons, QC luminescence has been extensively investigated for its potential application in high efficient plasma display and mercury-free fluorescent tubes [2–10]. Most recently, the research focus of QC has been shifted to near-infrared (NIR) region for its potential photovoltaic application [3]. The NIR-QC through down-conversion has been well demonstrated in Ln^{3+}–Yb^{3+} (Ln = Tb, Tm, Pr, Er and Ho) couples co-doped materials, which efficiently down-converts one incident UV-blue photon into two NIR photons (~1000 nm) via energy transfer (ET) from donor ions (Tb^{3+}, Tm^{3+}, Pr^{3+}, Er^{3+} and Ho^{3+}) to acceptor ions (Yb^{3+}) [11–18]. Yb^{3+} ion is well known to character the relatively simple two energy-level manifolds: the $^2F_{7/2}$ ground state and $^2F_{5/2}$ excited state at ~10,000 cm^{-1}. Its broad emission (900–1100 nm) is roughly overlapped with the band gap (1.12 eV) of crystalline silicon (c-Si), making Yb^{3+} as an attractive candidate for NIR-QC materials to improve the performance of c-Si solar cells [3,19]. However, in the most of the case, the NIR-QC are achieved through a second-order cooperative ET (CET, 10^3 times lower probable than the first-order resonant ET) [17,18,20], and the lower CET efficiency makes it only efficient at rather high Yb^{3+} concentration, where Yb^{3+} emission is mainly quenched due to concentration quenching (CQ) [3,11–17]. Thus, a NIR-QC via resonant ET process is more favorable for luminescent materials with a higher QE, which requires an intermediate level on donor ion to resonantly excite acceptor ions by the two-step ET processes.

In this paper, a feasible NIR-QC has been well demonstrated in Ho^{3+}–Yb^{3+} co-doped hexagonal β-$NaYF_4$ that efficiently converts one incident high-energy photon in 300–550 nm to two NIR photons. $NaYF_4$ was chosen as the host lattice due to its low phonon energy. Contrary to the typical upconversion scheme of $NaYF_4$:Ho^{3+},Yb^{3+} [20–22], the NIR-QC originating from the excited $^5F_3$ and from $^5S_2$,$^5F_4$ states of Ho^{3+} can be efficiently induced via the possible cooperative and resonant ET processes, respectively. Noted that low phonon energy is required for the both two fluoresce mechanisms because nonradiative relaxation (NR) from the $^5F_3$ and $^5S_2$,$^5F_4$ states is determined by multiphonon relaxation.

2. Experimental details

The $NaYF_4$:1%Ho^{3+},x%Yb^{3+} (x = 0, 1, 6, 10 and 20) phosphors were synthesized by a hydrothermal procedure using (Y_2O_3, Ho_2O_3, Yb_2O_3, 99.99% purity) and (HNO_3, NH_4HF_2, NaF, analytical reagent) as starting materials. Firstly, $Ln(NO_3)_3$ (Ln^{3+} = Y^{3+}, Ho^{3+} and Yb^{3+}) solutions (0.05 mol/L) were obtained by dissolving the specified stoichiometric Y_2O_3, Ho_2O_3 and Yb_2O_3 in a hot HNO_3 solution, respectively. Secondly, 0.005 mol NaF (0.2100 g) and 0.045 mol NH_4HF_2 (0.5668 g) were completely dissolved in distilled water, and then an appropriate amount of $Ln(NO_3)_3$ (Ln^{3+} = Y^{3+}, Ho^{3+} or Yb^{3+}) solution was added under magnetic stirring with adjusting the pH value to 3 by the dropwise of ammonia solution (27 wt.%). At last, after vigorous stirring for about 30 min, the resultant white suspension was transferred into a

* Corresponding author. Tel.: +86 20 87113681; fax: +86 20 87114204.
E-mail address: qyzhang@scut.edu.cn (Q.Y. Zhang).

0925-8388/$ – see front matter © 2011 Elsevier B.V. All rights reserved.
doi:10.1016/j.jallcom.2011.07.088

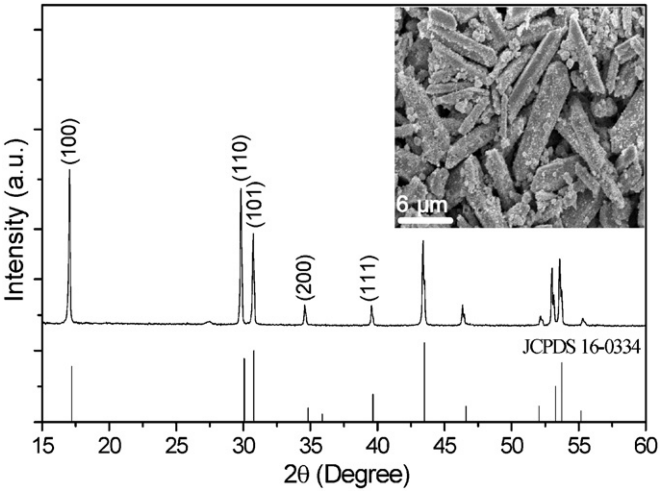

Fig. 1. The measured XRD pattern of $NaYF_4$:Ho^{3+},Yb^{3+} phosphors as well as the standard XRD pattern of $NaYF_4$ (JCPDS 16-0334) used as reference. Inset of Fig. 1 shows SEM image of the synthesized hexagonal $NaYF_4$:Ho^{3+},Yb^{3+} phosphors.

50 mL Teflon-lined stainless steel autoclave, filled up to 80% of its capacity, sealed tightly and heated at 220 °C in an electrical furnace for 20 h. After slowly cooled down to room temperature, the filtrated precipitate was centrifuged several times with the distilled water and absolute ethanol to remove any possible ionic remnant, and finally dried at 80 °C for 8 h in ambient atmosphere.

The phase identification of the obtained products was analyzed by means of a Philips Model PW1830 X-ray powder diffractometer (XRD) applying graphite monochromator and Cu *Kα* radiation (λ = 1.78010 Å). The size and morphology of the samples were inspected by a scanning electron microscope (SEM, JEOL JEM-1010). The photoluminescence (PL) and photoluminescence excitation (PLE) spectra, and fluorescence decay curves in visible and NIR regions were determined on a FSP920-combined with time resolved and steady state fluorescence spectrophotometer (Edinburgh Instruments LTD) fitted with a 450 W xenon lamp as the excitation source. All the visible PL spectra were corrected for the wavelength-dependent response of the detector system.

3. Results and discussion

3.1. Characterization

Fig. 1 shows the representative XRD pattern of the $NaYF_4$:Ho^{3+},Yb^{3+} sample and the standard XRD pattern (JCPDS 16-0334) of $NaYF_4$. It can be seen that the recorded XRD pattern is well indexed to a pure hexagonal *β*-$NaYF_4$ (primitive lattice, space group $p6_3/m$, $a = 5.96$ Å, $c = 3.53$ Å). There is no any other diffraction peak corresponding to impurity or allotropic phase, revealing the pure Ho^{3+}–Yb^{3+} co-doped *β*-$NaYF_4$ polycrystals have been obtained by the hydrothermal technique. The primitive unit cell of hexagonal *β*-$NaYF_4$ owns three cationic sites: one for Ln ions (1*a*), one for both Ln and sodium ions (1*f*), and the third for sodium ions (2 h) [23]. Because the ionic radius of Ho^{3+} (0.90 Å) or Yb^{3+} (0.86 Å) is very close to that of Y^{3+} (0.89 Å) [24], they would more probably substitute for the Y^{3+} ion with little defect. The SEM image of $NaYF_4$:Ho^{3+},Yb^{3+} microcrystals is exhibited in the inset of Fig. 1. It can be seen that the sample develops into typical hexagonal prismatic microrode with cracked ends. It is noted that the hexagonal *β*-$NaYF_4$ is a much better host lattice than the cubic *α*-$NaYF_4$ for the luminescence of various optically active Ln ions [23,25,26].

3.2. Cooperative NIR-QC in Ho^{3+}–Yb^{3+} couple from the excited Ho^{3+}:$^5F_3$ state

Upon 480 nm light exciting Ho^{3+} into the $^5F_3$ state in $NaYF_4$:Ho^{3+}, the typical PL peaks [Fig. 2(b)] centered at 540, 650, 750, 965 and 1015 nm can be strongly observed, which are easily attributed to the $^5F_4(^5S_2) \rightarrow {}^5I_8$, $^5F_5 \rightarrow {}^5I_8$, $^5F_4$,$^5S_2 \rightarrow {}^5I_7$, $^5F_5 \rightarrow {}^5I_7$ and $^5F_4$,$^5S_2 \rightarrow {}^5I_6$ transitions, respectively. Just as Yb^{3+} ions co-doped into $NaYF_4$:Ho^{3+}, the visible PL intensity of Ho^{3+} decreases monotonously with the Yb^{3+} content increase, while the intensity of NIR 985 nm emission (Yb^{3+}:$^2F_{5/2} \rightarrow {}^2F_{7/2}$) first rises up to the maximum at 10 mol%Yb^{3+} and then decreases due to CQ with further enhancement of Yb^{3+} content, as shown in Fig. 2(b). These results suggest that the excitation energy absorbed by Ho^{3+} ions can be efficiently transferred to Yb^{3+} ions in $NaYF_4$:Ho^{3+},Yb^{3+}. Accordingly, the well overlapping PLE bands [Fig. 2(a)], readily ascribed to the intra-4*f* forbidden transitions of Ho^{3+} ions, are recorded by monitoring the characteristic emissions of Ho^{3+} (540, 965 and 1015 nm) and Yb^{3+} (985 nm), respectively. These observation additionally provide a convinced proof for the efficient ET from Ho^{3+} to Yb^{3+} because there does not exist PLE band in 300–500 nm for Yb^{3+} ion (its charge transfer band located at shorter than 260 nm in $NaYF_4$ host) [27].

The energy level diagram in Fig. 3(a), labeled according to the Russell-Saunders Stark level structure of activator ions, schematically presents the possible ET processes of $Ho^{3+} \rightarrow Yb^{3+}$. Upon excitation of Ho^{3+} into the $^5F_3$ state, the strong NIR emission of Yb^{3+} can be obtained via the following three feasible ET mechanisms: (i) NIR-QC in Ho^{3+}–Yb^{3+} couple via a CET process: $Ho^{3+}(^5F_3) \rightarrow 2Yb^{3+}(^2F_{5/2}) + h\nu$; (ii) resonant cross-relaxation (CR) process following fast NR from the excited $^5F_3$ to $^5S_2$,$^5F_4$ states: $Ho^{3+}(^5S_2,{}^5F_4) + Yb^{3+}(^2F_{7/2}) \rightarrow Ho^{3+}(^5I_6) + Yb^{3+}(^2F_{5/2}) + h\nu$; (iii) another resonant CR process from $^5F_5$ state non-radiatively populated from higher energy levels: $Ho^{3+}(^5F_5) + Yb^{3+}(^2F_{7/2}) \rightarrow Ho^{3+}(^5I_7) + Yb^{3+}(^2F_{5/2}) + h\nu$. Though $NaYF_4$ host lattice owns a lower phonon energy ~400 cm^{-1}, the excited $^5F_3$ state can be nonradiatively decayed to the next $^5S_2$,$^5F_4$ states according to energy gap law [28], which is confidently proved by the intense 540 nm ($^5F_4$,$^5S_2 \rightarrow {}^5I_8$) and 750 nm ($^5F_4$,$^5S_2 \rightarrow {}^5I_7$) emissions [Fig. 3(b)]. Consequently, the last two ET mechanisms (ii) and (iii) are readily achieved by absorbing or emitting 1–2 phonons because of the roughly equal energy gaps: 9852 cm^{-1} (Ho^{3+}:$^5S_2$,$^5F_4 \rightarrow {}^5I_6$), 10,331 cm^{-1} (Ho^{3+}:$^5F_5 \rightarrow {}^5I_7$) and 10,000 cm^{-1} (Yb^{3+}:$^2F_{5/2} \rightarrow {}^2F_{7/2}$). However, just as the obvious PL band at 486 nm (Ho^{3+}:$^5F_3 \rightarrow {}^5I_8$) shown in Fig. 3(b), the excited $^5F_3$ state is testified to character lifetime long enough to compete with the multiphonon assisted NR processes. Furthermore, the PL intensity of 486 nm monotonously reduces according with Yb^{3+} content increase in $NaYF_4$:Ho^{3+},Yb^{3+}. These results directly indicate that the energy in the excited $^5F_3$ state can be efficiently transferred to the co-doping Yb^{3+} ions. That is to say, though the overlap between Ho^{3+} emission from the $^5F_3$ state and Yb^{3+} absorption is absent, the NIR-QC in Ho^{3+}–Yb^{3+} couple also can be reached by means of the second-order CET process because the sum of two Yb^{3+} (acceptor) absorption transitions energy equals to Ho^{3+} (donor) emission energy [7–11]. Therefore, the presence of Yb^{3+} ions as an extra decay pathway can efficiently compete with the spontaneous 486 nm emission ($^5F_3 \rightarrow {}^5I_8$) of Ho^{3+} ions.

Fluorescence decay curves of the Ho^{3+}:$^5F_3$ state are depicted in the inset of Fig. 3(b). It can be seen that the lifetime of the Ho^{3+}:$^5F_3$ level decreases slowly due to the inefficient $Ho^{3+} \rightarrow Yb^{3+}$ CET process at lower Yb^{3+} contents (≤10 mol%) but quickly due to the high efficient CET process at higher Yb^{3+} contents (>10 mol%), which well agrees with the nature of the second-order CET process. In this case, the total NIR QE is theoretically evaluated to be more than 100% [11–17]. However, as shown in Fig. 3(b), the PL intensity of the $^5F_3 \rightarrow {}^5I_8$ transition (486 nm) is proved to be rather weak by comparing with that of the $^5S_2$,$^5F_4 \rightarrow {}^5I_8$ transition (540 nm), which means that the excited $^5F_3$ state is almost completely depopulated to the following $^5S_2$,$^5F_4$ states by multiphonon relaxation. On the other hand, the CQ of Yb^{3+} NIR emission indeed occurs with Yb^{3+}

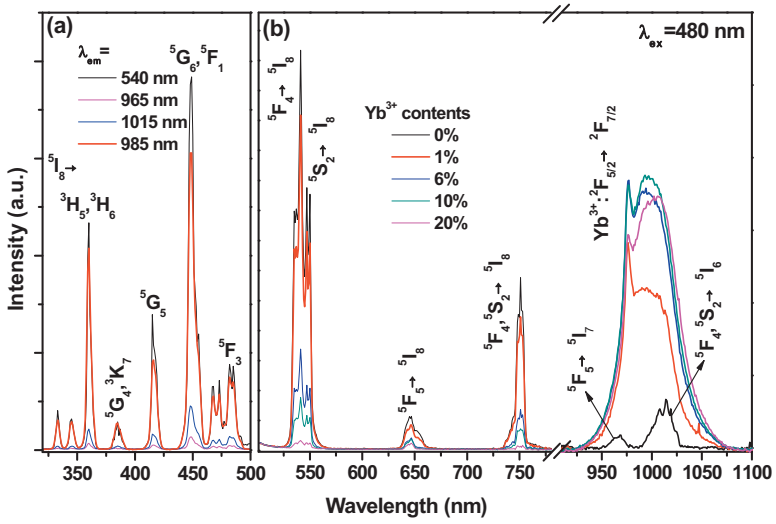

Fig. 2. (a) PLE spectra of the $NaYF_4$:Ho^{3+},Yb^{3+} phosphors, and (b) visible-NIR PL spectra (500–1100 nm) of the samples under excitation of 480 nm light.

concentration exceeding 10 mol%. Hence, the NIR-QC luminescence originating from the excited $^5F_3$ state is concluded to be relatively inefficient via CET from Ho^{3+} to Yb^{3+} ions.

3.3. *Efficient resonant NIR-QC in Ho^{3+}–Yb^{3+} couple with $^5I_6$ acting as an intermediate level*

When we record the NIR PL spectrum in a larger region, an intense NIR emission peak centered at 1180 nm (Ho^{3+}:$^5I_6 \rightarrow {}^5I_8$) can be observed upon excitation of Ho^{3+} into the $^5S_2$,$^5F_4$ states, as pictured in Fig. 4(b). It is of very significant interest to find that, under excitation of 535 nm light, not only the luminescence intensity of 985 nm enhances as Yb^{3+} doped into $NaYF_4$:Ho^{3+}, but also that of Ho^{3+}:$^5I_6 \rightarrow {}^5I_8$ transition (1180 nm) monotonously increases. Inversely, the visible luminescence intensity of Ho^{3+}, as shown in Fig. 4(b), quickly decreases with the addition of Yb^{3+} ions, suggesting that ET efficiently takes place from Ho^{3+} to Yb^{3+}. Fig. 4(a) exhibits the PLE spectra of $NaYF_4$:Ho^{3+},Yb^{3+} monitored at emission lights of Ho^{3+} (650 and 1180 nm) and Yb^{3+} (985 nm), respectively. The measured PLE bands in 300–550 nm, well assigned to the corresponding intra-4*f* transition of Ho^{3+}, overlap well with each other, which further provide a convinced evidence for the efficient ET from Ho^{3+} to Yb^{3+}.

The ET process of $NaYF_4$:Ho^{3+},Yb^{3+} has been schematically illustrated in an energy level diagram plotted in Fig. 5(a). Upon excitation of Ho^{3+} into the $^5S_2$,$^5F_4$ states, the resonant two-step NIR-QC in Ho^{3+}–Yb^{3+} couple can efficiently occur with the $^5I_6$ state acting as an intermediate level: firstly, the excited Ho^{3+}:$^5S_2$,$^5F_4$ states can intensely excite one Yb^{3+} neighbor through a resonant CR process (Ho^{3+}:$^5S_2$,$^5F_4 \rightarrow {}^5I_6$ and Yb^{3+}:$^2F_{7/2} \rightarrow {}^2F_{5/2}$) emitting a NIR 985 nm photon, and secondly, the populated $^5I_6$ state can be sequentially decay to the $^5I_8$ ground state by generating another NIR 1180 nm photon. As a result, the Yb^{3+} luminescence intensity enhances with Yb^{3+} contents increase due to the more efficient resonant CR between Ho^{3+} and Yb^{3+} at higher Yb^{3+} concentration but reduces at Yb^{3+} contents more than 10 mol% due to CQ among Yb^{3+} ions. On the other hand, the 1180 nm PL intensity of Ho^{3+} also improves greatly because of the more population of $^5I_6$ state induced by the more efficient resonant CR between Ho^{3+} and Yb^{3+} at higher Yb^{3+} contents. Because the probability of the

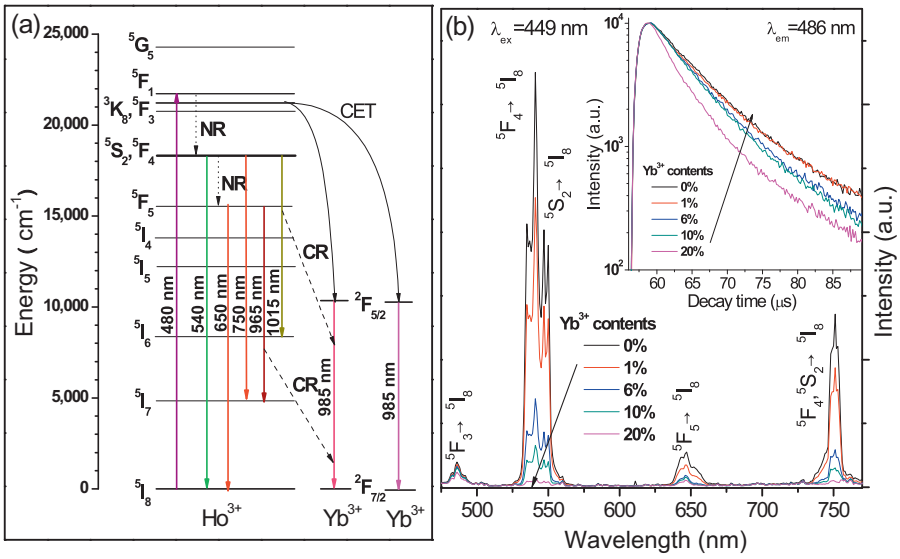

Fig. 3. (a) Schematic energy level diagram indicating the CET process of $Ho^{3+} \rightarrow Yb^{3+}$, and (b) visible PL spectra (λ_{ex} = 449 nm) of Ho^{3+} as a function of Yb^{3+} contents. The inset of Fig. 3(b) exhibits the decay curves of the Ho^{3+}:$^5F_3 \rightarrow {}^5I_8$ transition in $NaYF_4$:Ho^{3+},Yb^{3+}.

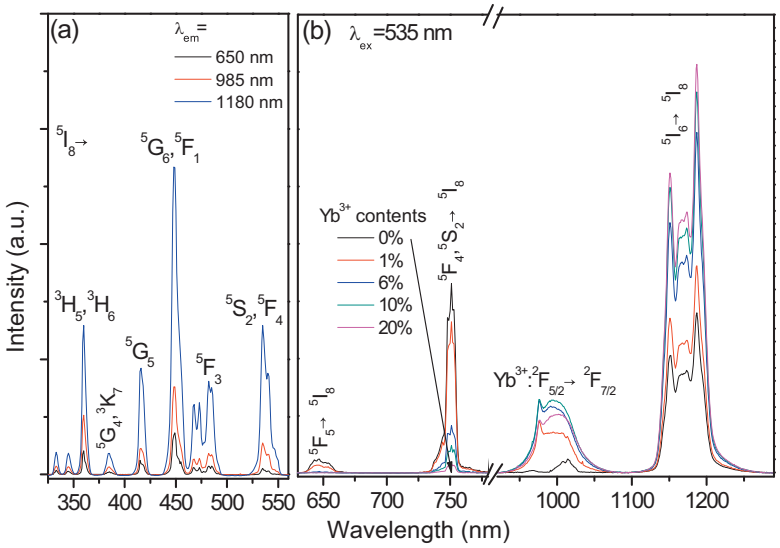

Fig. 4. (a) PLE spectra of $NaYF_4$:Ho^{3+},Yb^{3+} monitored at PL of 650, 985 and 1180 nm, respectively, and (b) PL spectra (λ_{ex} = 535 nm) in the wavelength region of 610–1290 nm.

first-order resonant ET process is typically 10^3 higher than that of the second-order CET process [20], this resonant NIR-QC in Ho^{3+}–Yb^{3+} couple should be considerably efficient to sequentially emit a 985 and 1180 nm photon by down-converting a high-energy photon absorbed in the wavelength region of 300–550 nm.

The decay curves of the Ho^{3+}:$^5S_2$,$^5F_4$ states are depicted in Fig. 5(b) for the samples doped with various Yb^{3+} contents. A mean decay time τ_m is given by the following equation:

$$\tau_m = \int_{t_0}^{\infty} \left[\frac{I_{(t)}}{I_0}\right] dt, \quad (1)$$

where $I_{(t)}$ is the luminescence intensity depending on time t and I_0 is the maximum value of $I_{(t)}$, which occurs at the initial time t_0 [29]. For the Yb^{3+}-free sample, a nearly single exponential decay curve is obtained with a lifetime of 160.49 μs. As Yb^{3+} contents increase, the decay curves turn to be nonexponential with a rapid decrease in lifetime, which can be explained by the introduction of an extra decay pathway, *i.e.*, the resonant ET from the excited Ho^{3+} to neighboring Yb^{3+} ions, efficiently competing with the spontaneous emission (540 nm) of Ho^{3+} ions. The ET efficiency is defined as the ratio of donor ions that are depopulated by ET to acceptor ions over the total number of excited donor ions [3–11]. Supposing that there does not exist nonradiative energy losses by defects and impurities, the ET efficiency (η_{ET}) and the total QE (η_{QE}) of $NaYF_4$:Ho^{3+},Yb^{3+} phosphors can be theoretically calculated by the following equations [1–3,11–17]:

$$\eta_{ET} = \eta_{x\%Yb} = 1 - \frac{\int I_{x\%Yb}\,dt}{\int I_{0\%Yb}\,dt}, \quad (2)$$

$$\eta_{QE} = \eta_{Ho}(1 - \eta_{ET}) + 2\eta_{Yb}\eta_{ET}, \quad (3)$$

where I denotes the decay intensity, x% Yb denotes the Yb^{3+} contents, and η_{Ho} and η_{Yb} stand for QE of Ho^{3+} and Yb^{3+}. It has been determined that the η_{ET} for the samples doped with 1, 6, 10 and 20 mol% Yb^{3+} are 17%, 68%, 82% and 86% respectively. Correspondingly, on the assumption that all the excited Ho^{3+} and Yb^{3+} decay radiatively, *i.e.*, $\eta_{Yb} = \eta_{Ho} = 1$, the upper limits values of η_{QE} can be

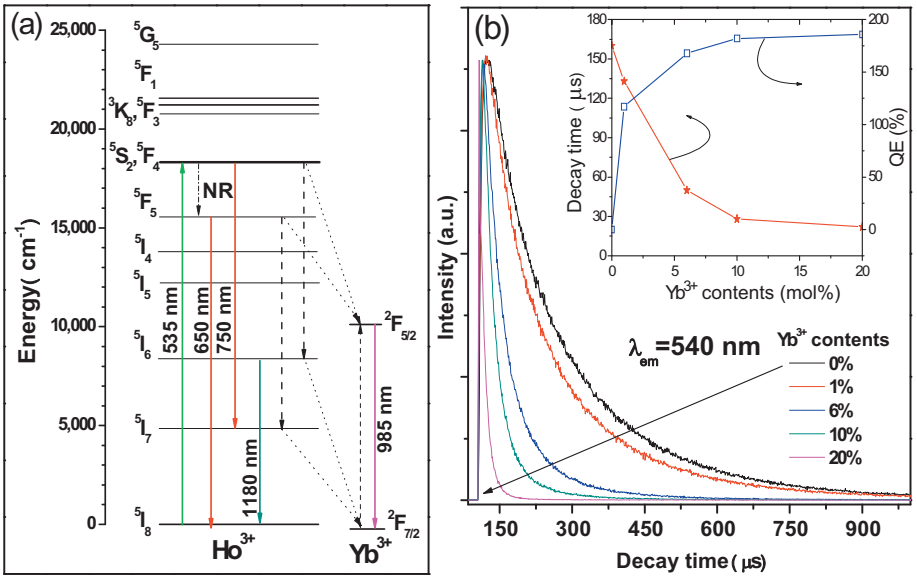

Fig. 5. (a) Schematic energy levels of Ho^{3+}–Yb^{3+} couple illustrating the resonant NIR-QC process, and (b) the decay curves of Ho^{3+}:$^5S_2$,$^5F_4$ PL (540 nm). The inset of (b) shows the dependence of decay time and NIR QE on Yb^{3+} contents for $NaYF_4$:Ho^{3+},Yb^{3+}.

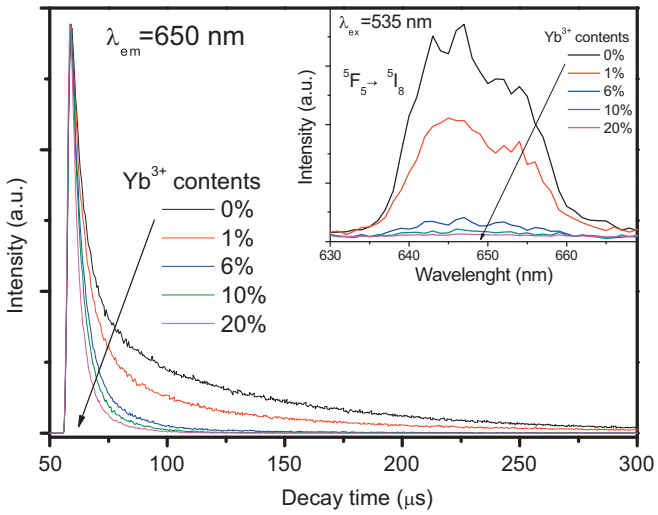

Fig. 6. Decay curves of Ho^{3+}:$^5F_5$ PL (650 nm) in $NaYF_4$:Ho^{3+},Yb^{3+}. The inset shows the Yb^{3+} contents dependent Ho^{3+}:$^5F_5 \rightarrow {}^5I_8$ luminescence spectra (λ_{ex} = 535 nm).

estimated to be 117%, 168%, 182% and 186%. Additionally, the decay time and QE as a function of Yb^{3+} contents are shown in the inset of Fig. 5(b). It is noted that, although NIR emission (985 nm) is quenched due to CQ at Yb^{3+} contents beyond 10 mol%, the exact maximum QE is still up to 182%.

However, as indicated in Fig. 5(a), another resonant CR process between Ho^{3+}:$^5F_5 \rightarrow {}^5I_7$ and Yb^{3+}:$^2F_{7/2} \rightarrow {}^2F_{5/2}$ also contribute to the intense 985 nm photons emission at a certain extent. Just as shown in Fig. 6, the decay time of Ho^{3+}:$^5F_5$ state quickly decreases with the Yb^{3+} content increase, revealing the existence of ET from Ho^{3+} to Yb^{3+}. More importantly, as shown in the inset of Fig. 6, the Yb^{3+} contents dependent Ho^{3+}:$^5F_5 \rightarrow {}^5I_8$ luminescence spectra further confirm that $Ho^{3+}(^5F_5) + Yb^{3+}(^2F_{7/2}) \rightarrow Ho^{3+}(^5I_7) + Yb^{3+}(^2F_{5/2})$ resonant CR process does play a certain role in improving the NIR PL intensity of Yb^{3+} ions, especially at higher Yb^{3+} contents in $NaYF_4$:Ho^{3+},Yb^{3+}. However, for the large energy gap ~3100 cm^{-1} of $^5S_2$,$^5F_4 \rightarrow {}^5F_5$ but low phonon energy ~400 cm^{-1} of $NaYF_4$ host lattice, the $^5F_5$ state populated by multiphonon assisted NR from the upper excited $^5S_2$,$^5F_4$ states is demonstrated to be rather inefficient by comparing the PL intensity of 540 or 750 nm with that of 650 nm. Hence, it can be concluded that the first-order resonant NIR-QC from the Ho^{3+}:$^5S_2$,$^5F_4$ states would dominate the NIR photons emission in $NaYF_4$:Ho^{3+},Yb^{3+} phosphors.

4. Conclusion

In summary, efficient NIR-QC in $NaYF_4$:Ho^{3+},Yb^{3+} has been well demonstrated via the cooperative and resonant ET processes from Ho^{3+} to Yb^{3+} ions. The high-energy photons of 300–550 nm are facilitated to be down-converted to NIR photons by a factor of 2. The fluorescence decay times of Ho^{3+} donors are recorded under excitation of Ho^{3+} into various states as a function of Yb^{3+} concentration. As expected, the first-order resonant NIR-QC process is determined to dominate the intense NIR emissions of 985 nm (Yb^{3+}) and 1180 nm (Ho^{3+}) and an optimum QE is rationally estimated to be about 182% before Yb^{3+} reaching the CQ threshold. This efficient NIR-QC material may significantly improve the potential application in increasing the performance of solar cells.

Acknowledgements

This work is financially supported by the NSFC (Grant Nos. 50872036 and U0934001), and the Fundamental Research Funds for the Central Universities, SCUT.

References

[1] D.L. Dexter, Phys. Rev. 108 (1957) 630–633.
[2] R.T. Wegh, H. Donker, K.D. Oskam, A. Meijerink, Science 282 (1999) 663–666.
[3] Q.Y. Zhang, X.Y. Huang, Prog. Mater. Sci. 55 (2010) 353–427.
[4] W.W. Piper, J.A. de Luca, F.D. Ham, J. Lumin. 8 (1974) 344–348.
[5] J.L. Sommerdijk, A. Bril, A.W. de Jager, J. Lumin. 8 (1974) 341–343.
[6] R. Pappalardo, J. Lumin. 14 (1976) 159–193.
[7] C. Feldmann, T. Juster, C.R. Ronda, P.J. Schmidt, Adv. Funct. Mater. 13 (2003) 511–516.
[8] A.M. Srivastava, W.W. Beers, J. Lumin. 71 (1997) 285–290.
[9] A.N. Belsky, N.M. Khaidukov, J.C. Krupa, V.N. Makhov, A. Philipov, J. Lumin. 94-95 (2001) 45–49.
[10] S.M. Loureiro, A. Setlur, W. Heward, S.T. Taylor, H. Comanzo, P. Schmidt, U. Happek, Chem. Mater. 17 (2005) 3108–3113.
[11] P. Vergeer, T.J.H. Vlugt, M.H.F. Kox, M.I. Den Hertog, J.P.J.M. van der Eerden, A. Meijerink, Phys. Rev. B 71 (2005) 014119–014129.
[12] Q.Y. Zhang, C.H. Yang, Y.X. Pan, Appl. Phys. Lett. 90 (2007) 021107.
[13] Q.Y. Zhang, C.H. Yang, Z.H. Jiang, X.H. Ji, Appl. Phys. Lett. 90 (2007) 061914.
[14] G. Lakshminarayana, J.R. Qiu, J. Alloys Compd. 481 (2009) 582–589.
[15] Q.Y. Zhang, G.F. Yang, Z.H. Jiang, Appl. Phys. Lett. 91 (2007) 051903.
[16] B.M. van der Ende, L. Aarts, A. Meijerink, Adv. Mater. 21 (2009) 3073–3077.
[17] H. Lin, D.Q. Chen, Y.L. Yu, A.P. Yang, Y.S. Wang, Opt. Lett. 36 (2011) 876–878.
[18] J.J. Eilers, D. Biner, J.T. Van Wijngaarden, K. Krämer, H.-U. Güdel, A. Meijerink, Appl. Phys. Lett. 96 (2010) 151106.
[19] B.S. Richards, Sol. Energy Mater. Sol. Cells 90 (2006) 1189–1207.
[20] F. Auzel, Chem. Rev. 104 (2004) 139–173.
[21] X.F. Wang, S.G. Xiao, Y.Y. Bu, J.W. Bing, J. Alloys Compd. 477 (2009) 941–945.
[22] M.M. Xing, W.H. Cao, H.Y. Zhong, Y.H. Zhang, X.X. Luo, Y. Fu, W. Feng, T. Pang, X.F. Yang, J. Alloys Compd. 509 (2011) 5725–5730.
[23] C.X. Li, Z.W. Quan, J. Yang, P.P. Yang, J. Lin, Inorg. Chem. 46 (2007) 6329–6337.
[24] R.D. Shannon, Acta Cryst. A 32 (1976) 751–766.
[25] K.W. Krämer, D. Biner, G. Frei, H.U. Güdel, M.P. Hehlen, S.R. Lüthi, Chem. Mater. 16 (2004) 1244–1251.
[26] S. Heer, K. Krömpe, H.-U. Güdel, M. Haase, Adv. Mater. 16 (2004) 2102–2104.
[27] E. van der Kolk, O.M. Ten Kate, J.W. Wiegman, D. Biner, K.W. Krämer, Opt. Mater. 33 (2011) 1024–1027.
[28] J.M.F. van Dijk, M.F.H. Schuurmans, J. Chem. Phys. 78 (1983) 5317–5323.
[29] E. Nakazawa, in: S. Shionoya, W.M. Yen (Eds.), Phosphor Handbook, CRS Press, 1999, pp. 102–104 (Chapter 2).